Journal of Materiomics 5 (2019) 88–93

Contents lists available at ScienceDirect

Journal of Materiomics

journal homepage: www.journals.elsevier.com/journal-of-materiomics/

# Influence of Bi on the thermoelectric properties of $SrTiO_{3-\delta}$

Cong Chen [a, b, *], Mohamed Bousnina [a], Fabien Giovannelli [a], Fabian Delorme [a]

[a] Université de Tours, CNRS, INSA CVL, GREMAN UMR 7347, IUT de Blois, 15 rue de la chocolaterie, CS 2903, 41029, Blois Cedex, France
[b] Bundesanstalt für Materialforschung und −prüfung (BAM), Unter den Eichen 87, 12205, Berlin, Germany

ARTICLE INFO

*Article history:*
Received 15 September 2018
Received in revised form
4 December 2018
Accepted 14 December 2018
Available online 15 December 2018

*Keywords:*
Thermoelectrics
$SrTiO_3$
Composite
Bi
Magnéli phase

ABSTRACT

The thermoelectric properties of $Sr_{1-x}Bi_xTiO_{3-\delta}$ ($0 \le x \le 0.07$) have been investigated. Dense ceramics of $Sr_{1-x}Bi_xTiO_{3-\delta}$ and $Sr_{0.95}TiO_{3-\delta}$ have been prepared by solid-state reaction and conventional sintering in air followed by annealing in a reducing atmosphere. XRD and SEM analyses show that the rutile $TiO_2$ in $Sr_{0.95}TiO_3$ formed after sintering becomes Magnéli phase of $Ti_nO_{2n-1}$ after annealing. Moreover, Bi resolves from $Sr_{1-x}Bi_xTiO_3$ after annealing, resulting in the formation of $Sr_{1-x}Bi_xTiO_{3-\delta}/Bi/Ti_nO_{2n-1}$ composites. With increasing Bi content in $Sr_{1-x}Bi_xTiO_{3-\delta}$, the electrical conductivity increases while the absolute values of the Seebeck coefficient decrease as a result of increasing carrier concentration. The thermal conductivity of $SrTiO_{3-\delta}$ is reduced by doping Bi up to $x = 0.07$. Highest $ZT$ ~0.13 is obtained in $Sr_{0.93}Bi_{0.07}TiO_{3-\delta}$ at 1000 K.


## 1. Introduction

Oxide thermoelectric materials have the advantages of low cost, low toxicity, and good chemical stability at high temperatures. High-performance p-type thermoelectric oxides include layered cobalt oxides containing 2D edge sharing $CoO_6$ octahedra [1–6] and acceptor-doped perovskite $LaCoO_3$ [7–10], while n-type oxides include donor-doped $SrTiO_3$ [11–13], $CaMnO_3$ [14], Al-doped ZnO [15,16], etc. Among them, donor-doped $SrTiO_3$ exhibits a large Seebeck coefficient due to a large carrier effective mass and the orbital degeneracy of Ti 3d-$t_{2g}$ conduction band [11]. Its electrical conductivity can be tuned from insulating to metallic through substitutional doping and/or introducing oxygen deficiency. Usually, $SrTiO_3$ is sintered under a reducing atmosphere and doped with rare-earth elements on $Sr^{2+}$ sites and/or $Nb^{5+}$ on $Ti^{4+}$ sites [17–19]. By adjusting dopants and doping concentration, the electrical conductivity can be improved due to increased carrier concentration, while the lattice thermal conductivity can be reduced by strain field scattering, mass fluctuation and point defects [20,21].

High figure of merit ($ZT$) values in the range of 0.30–0.41 have been reported in $SrTiO_3$ substituted by 8% La and 12% Dy (double substitution) [22], 10% Pr with A-site deficiency [23], 10% Y [24], 10%–15% Nb [25], 15% La and A-site vacancies [26], etc. Moreover, similar high $ZT$ values have been achieved in composites consisting of La/Nb doped $SrTiO_3$ and Cu/Fe [27]. However, the $ZT$ values of doped $SrTiO_3$ are still low compared to traditional thermoelectric materials owing to its high lattice thermal conductivity. Therefore, nanostructuring approaches have been adopted to enhance the phonon scattering, such as synthesizing $SrTiO_3$ nanoparticles [28], introducing nanoinclusions [29,30], and fabricating $SrTiO_3$ superlattices [31], etc. Moreover, Ruddlesden-Popper (RP) phases of $SrO(SrTiO_3)_n$ with a layered crystal structure have been investigated [32,33]. Although a decrease in the thermal conductivity is achieved in the RP phases, the electrical conductivity also decreases due to the insulating SrO layers, resulting in lower values of $ZT$ than donor-doped $SrTiO_3$.

In this work, we aim to investigate the effect of $Bi^{3+}$ substitution on the thermoelectric properties of $SrTiO_{3-\delta}$. By replacing $Sr^{2+}$ with $Bi^{3+}$, we intend to i) improve the electrical conductivity by increased carrier concentration, and ii) reduce the lattice thermal conductivity due to the large mass difference between $Bi^{3+}$ and $Sr^{2+}$. Gong et al. reported that a $ZT$ value of 0.269 at 1073 K can be achieved in La- and Bi-codoped $SrTiO_3$ [34]. However, it is not clear whether the improved thermoelectric properties are due to La or Bi. Therefore, it is necessary to study $SrTiO_3$ with a single type of dopant, Bi. This paper reports the thermoelectric properties of $Sr_{1-x}Bi_xTiO_{3-\delta}$ ($0 \le x \le 0.07$) and $Sr_{0.95}TiO_{3-\delta}$ in the temperature range of

* Corresponding author. Bundesanstalt für Materialforschung und −prüfung (BAM), Unter den Eichen 87, 12205, Berlin, Germany.
*E-mail address:* saracongchen@gmail.com (C. Chen).
Peer review under responsibility of The Chinese Ceramic Society.

https://doi.org/10.1016/j.jmat.2018.12.004

300 K–1000 K, synthesized by solid-state reaction and conventional sintering.

## 2. Experiment

Powders of $Sr_{1-x}Bi_xTiO_3$ ($x = 0$, 0.005, 0.01, 0.03, 0.05, and 0.07) and $Sr_{0.95}TiO_3$ were synthesized by solid state reaction. Stoichiometric amounts of $SrCO_3$ (Sigma Aldrich, ≥ 98%), $Bi_2O_3$ (Acros Organics, ≥ 99.9%), and $TiO_2$ (Sigma Aldrich, ≥ 99.9%) powders were mixed by planetary ball mill (RETSCH PM100) at 250 rpm for 5 min with a tungsten carbide jar and beads. The powder mixture was pelletized by a uniaxial pressing machine and calcined at 1373 K for 2 h over $ZrO_2$ beads in an alumina crucible in air. The pellets were ball milled again at 250 rpm for 5 min. The powder was pressed into pellets and sintered at 1673 K for 2 h over $ZrO_2$ beads in an alumina crucible in air, followed by annealing at 1673 K for 12 h in a reducing atmosphere (67%$N_2$/30%Ar/3%$H_2$).

Room-temperature X-ray diffraction (XRD) was performed by a BRUKER D8 Advance θ/2θ diffractometer equipped with a Linxeye energy-dispersive one-dimensional detector, with Cu-Kα radiation and operating at 40 kV and 40 mA. Scans were recorded from 20° to 85° (2θ) with a step of 0.02° and a counting time of 0.5 s per step. Rietveld refinement was carried out using Fullprof Suite [35]. Microstructure was examined by scanning electron microscopy (SEM, Tescan MIRA3) coupled with a backscattered electron detector (BSD) and an energy-dispersive X-ray spectroscopy (EDS, Oxford INCA X-act). Samples were gold-coated by sputtering prior to observation.

Electrical conductivity and Seebeck coefficient were measured simultaneously by ULVAC ZEM3 in a low pressure He atmosphere from a high of 1000 K to a low of 323 K. Points of contact between samples and two thermocouples were coated with a thin layer of gold to reduce the contact resistance. Thermal conductivity is a product of density, thermal diffusivity, and specific heat capacity. Bulk density was determined from the dry mass and the geometric dimensions of pellets. Graphite coating was applied on the samples for thermal diffusivity measurement (Netzsch LFA457). It was performed from 373 K to 1000 K in vacuum and the data were average values of three measurements at each temperature. Specific heat capacity was measured from room temperature up to 1000 K, with a heating rate of 20 $K.min^{-1}$ in platinum crucibles in a nitrogen atmosphere (NETZSCH STA449 F3).

## 3. Results and discussion

Fig. 1a shows that $Sr_{1-x}Bi_xTiO_3$ ($0 \le x \le 0.07$) ceramics exhibit cubic $SrTiO_3$ phase (PDF 00-035-0734) with a space group *Pm*-3m after sintering in air. The intensity is plotted in a logarithmic scale to emphasize the impurity peaks. $Sr_{0.95}TiO_3$ contains an additional rutile $TiO_2$ phase (PDF 00-021-1276). A satellite peak next to the (110) peak has been observed in every composition, probably corresponding to $Sr_2TiO_4$, which may appear as an impurity phase during synthesis of $SrTiO_3$ [36]. It is noticed that some samples show a minor diffraction peak at ~28° and that $Sr_{0.95}TiO_3$ after sintering in air shows one at ~44°. However, it is difficult to determine the phases correctly due to their low intensities and limited number of peaks present. After annealing in a reducing atmosphere (Fig. 1b), diffraction peaks corresponding to Bi metal (PDF 01-079-6675) appear at 2θ of 27.19° and 37.99° in $Sr_{1-x}Bi_xTiO_{3-\delta}$ with $x = 0.05$ and 0.07 and their diffraction intensity increases with increasing *x*. Bi metal does not seem to exist in the compositions with lower Bi content. It means that the solubility (or substitution) limit of Bi in $SrTiO_3$ is lower than 5 at. %, or that we are below the XRD detection threshold. Moreover, the diffraction peaks corresponding to rutile $TiO_2$ can no longer be observed in the XRD pattern of $Sr_{0.95}TiO_{3-\delta}$. All ceramics show densities over 93% of the theoretical density of $SrTiO_3$ calculated from the Rietveld refinements, which are dense enough for the measurement of thermoelectric properties.

The XRD patterns as shown in Fig. 1 are refined to calculate lattice parameters. Fig. 2a and b show two examples of the refined XRD patterns of $Sr_{1-x}Bi_xTiO_{3-\delta}$ with $x = 0$ and 0.05 after annealing in a reducing atmosphere. The poor Rietveld refinement in Fig. 2b is probably due to the presence of the above-mentioned impurities. The lattice parameter *a* of the air-sintered and reducing atmosphere-annealed samples is shown in Fig. 2c. In both cases, the lattice parameter of $Sr_{1-x}Bi_xTiO_{3-\delta}$ increases with increasing Bi content, although the ionic radius of $Sr^{2+}$ (1.26 Å) is larger than that of $Bi^{3+}$ (1.17 Å) [37]. As the ionic radius for $Bi^{3+}$ in twelve-fold coordination is not available, the ionic radii in eight-fold coordination for both ions are used here. The unit cell expansion could be attributed to the formation of oxygen vacancies and $Ti^{3+}$ ions. Oxygen vacancy induces an increase in the Coulomb repulsion between neighboring transition metals ions, thus increasing unit cell volume. Moreover, the extra charge induced by $Bi^{3+}$ substitution and oxygen vacancies could be compensated by partial reduction of $Ti^{4+}$ (0.605 Å) into $Ti^{3+}$ (0.67 Å) [37]. The lattice parameters of the reducing atmosphere-annealed samples are larger than those of the air-sintered samples at each Bi content, which is most probably due to increased oxygen deficiency. The lattice parameters of air-sintered and reducing atmosphere-annealed $Sr_{0.95}TiO_3$ are similar to the undoped $SrTiO_3$ and less than the Bi-doped samples, indicating the existence of Bi dopant in the crystal structure of $Sr_{1-x}Bi_xTiO_{3-\delta}$ in spite of the appearance of Bi metal.

Fig. 3 shows SEM and BSD images of a fracture surface of the annealed $Sr_{1-x}Bi_xTiO_{3-\delta}$ ceramic with $x = 0.01$. XRD only shows the existence of Bi metal in the composition with $x = 0.05$ and 0.07. It is not known whether the absence of diffraction peaks corresponding to Bi metal in $Sr_{1-x}Bi_xTiO_{3-\delta}$ with $x < 0.05$ is due to that it is below the solubility of Bi or detection limit of the XRD instrument. Therefore, the microstructure of the composition with $x = 0.01$ was examined. The BSD image shows a clear contrast between different phases. The atomic ratio between different elements from EDS analysis is shown in the insert of Fig. 3. The light grey area shows a similar atomic ratio between Sr and Ti, indicating that it is most likely $SrTiO_3$. The bright spots are rich in Bi, while the liquid-like dark areas are rich in Ti. Therefore, Bi metal exists in $Sr_{1-x}Bi_xTiO_{3-\delta}$ even at a Bi content lower than what has been indicated in the XRD analysis (Fig. 1b). It is ascribed to the decomposition of $Sr_{1-x}Bi_xTiO_{3-\delta}$ after annealing at 1673 K under a reducing atmosphere, in agreement with a previous study on the degradation of $SrBi_2Ta_2O_9$ in which $SrBi_2Ta_2O_9$ decomposes into Bi metal and Sr-Ta oxide above 573 K under 4%$H_2$/Ar atmosphere [38]. Bi metal and Ti-rich phase have also been observed in $Sr_{1-x}Bi_xTiO_{3-\delta}$ ceramics with other Bi contents. The Ti-rich phase is Magnéli phase ($Ti_nO_{2n-1}$), a commonly found phase in Sr deficient $SrTiO_3$ [39]. As Bi leaves the lattice site, $Sr_{1-x}Bi_xTiO_{3-\delta}$ becomes A-site deficient and $Ti_nO_{2n-1}$ is formed. $Ti_nO_{2n-1}$ is also observed in $Sr_{0.95}TiO_{3-\delta}$ as a result of excess $TiO_2$. It is believed that above the solubility limit of Sr vacancy in the $SrTiO_3$ structure, $Ti_nO_{2n-1}$ will form as a secondary phase in a reducing atmosphere.

Fig. 4a and b show the temperature dependence of the electrical conductivity and Seebeck coefficient of $Sr_{1-x}Bi_xTiO_{3-\delta}$ and $Sr_{0.95}TiO_{3-\delta}$. $Sr_{1-x}Bi_xTiO_{3-\delta}$ with $0 \le x \le 0.005$ shows semiconducting electrical conductivity over the whole range of temperature, while the samples with $0.01 \le x \le 0.07$ show metallic conduction above 400 K. The electrical conductivity of $Sr_{1-x}Bi_xTiO_{3-\delta}$ increases with increasing Bi content up to $x = 0.05$. All compositions are n-type, as they possess negative values of Seebeck coefficient. In general, the absolute values of Seebeck coefficient

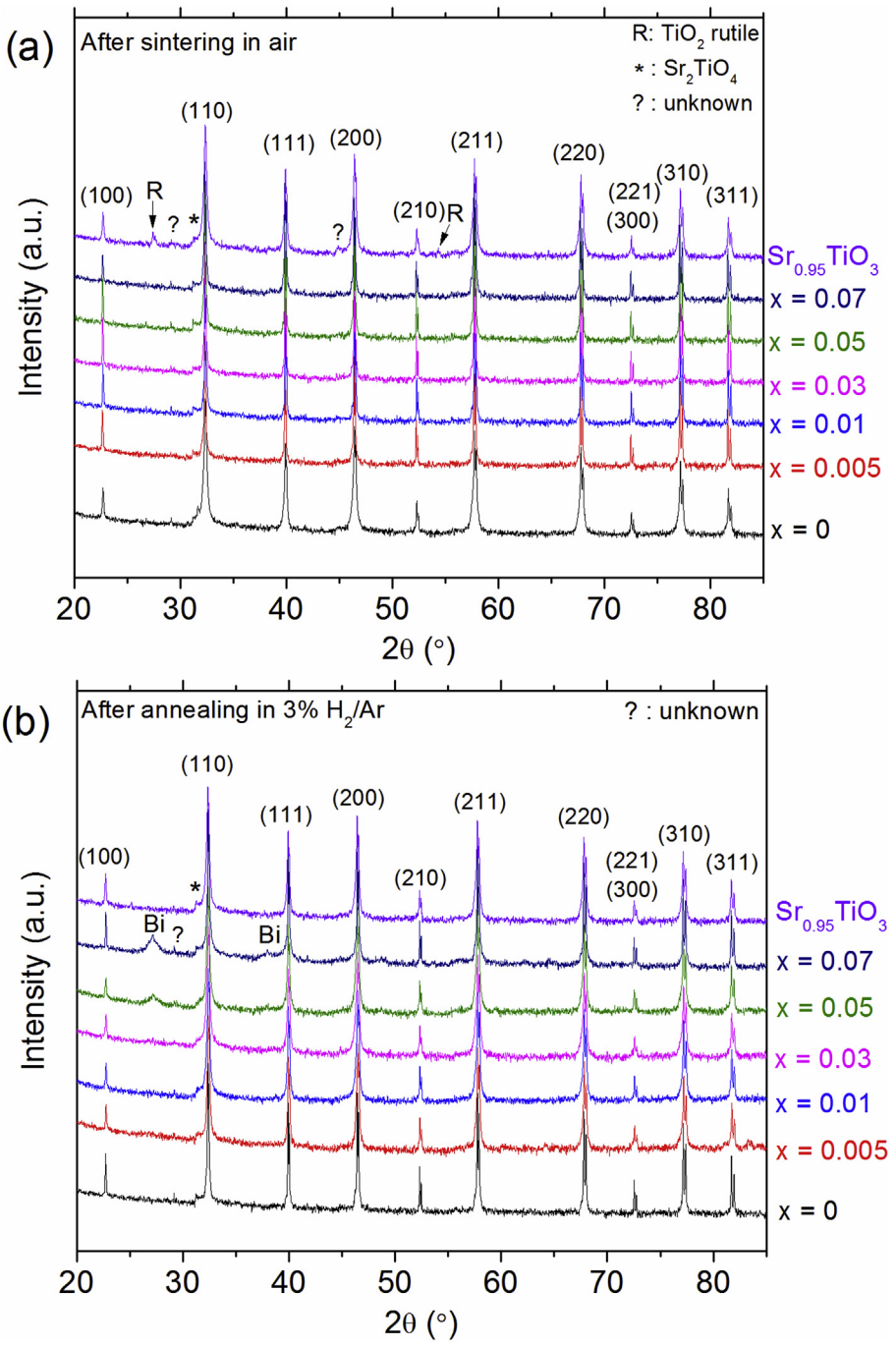


**Fig. 1.** X-ray diffraction patterns of $Sr_{1-x}Bi_xTiO_{3-\delta}$ ($x = 0$, 0.005, 0.01, 0.03, 0.05, and 0.07) and $Sr_{0.95}TiO_{3-\delta}$ ceramics (a) after sintering in air and (b) after annealing in a reducing atmosphere. Letter R, star (*), question mark (?), and Bi indicate diffraction peaks corresponding to rutile $TiO_2$, $Sr_2TiO_4$, unknown phases and Bi metal, respectively.

decrease with increasing Bi until $x = 0.05$. An increase in the carrier concentration via Bi substitution is confirmed by the simultaneous increase in electrical conductivity and decrease in the absolute values of Seebeck coefficient. $Sr_{0.95}TiO_{3-\delta}$ has been synthesized to confirm the role of Bi substitution and $Ti_nO_{2n-1}$ in $SrTiO_{3-\delta}$. Compared to $SrTiO_{3-\delta}$, $Sr_{0.95}TiO_{3-\delta}$ possesses higher electrical conductivity and lower absolute values of Seebeck coefficient, possibly due to the presence of $Ti_nO_{2n-1}$ in $Sr_{0.95}TiO_{3-\delta}$. $Ti_nO_{2n-1}$ is a series of n-type thermoelectric materials and possesses better thermoelectric performance than the undoped $SrTiO_{3-\delta}$ in this work [40,41]. Therefore, the incorporation of $Ti_nO_{2n-1}$ in $SrTiO_{3-\delta}$ could improve its electrical conductivity and reduce its absolute values of Seebeck coefficient. On the other hand, $Sr_{0.95}TiO_{3-\delta}$ shows a much lower electrical conductivity than $Sr_{0.95}Bi_{0.05}TiO_{3-\delta}$. It could be due to its low carrier concentration and probably low mobility. It is clear from Fig. 2c that the lattice parameter of $Sr_{0.95}TiO_{3-\delta}$ is similar to the undoped $SrTiO_{3-\delta}$ and smaller than all of the Bi-doped samples, indicating a lack in the carrier concentration contributed by Bi substitution and oxygen deficiency. Moreover, below a critical carrier concentration, the carrier mobility of $SrTiO_{3-\delta}$ decreases with decreasing carrier concentration [42]. Finally, the Seebeck coefficient of the samples presents a very complex behaviour, with

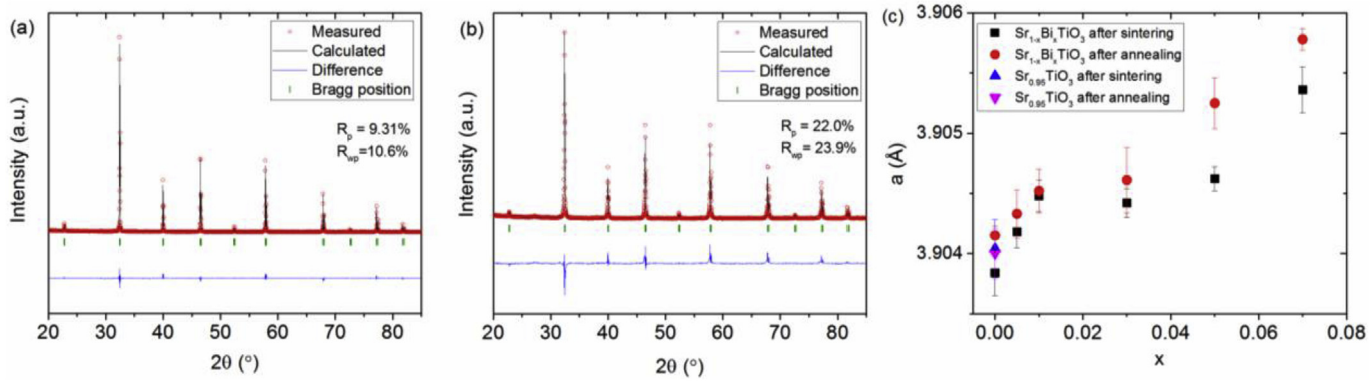


**Fig. 2.** Examples of Rietveld refinement of $Sr_{1-x}Bi_xTiO_{3-\delta}$ ceramics after annealing in a reducing atmosphere with a composition (a) $x = 0$ and (b) $x = 0.05$. (c) Lattice parameter $a$ of $Sr_{1-x}Bi_xTiO_{3-\delta}$ ($x = 0$, 0.005, 0.01, 0.03, 0.05, and 0.07) and $Sr_{0.95}TiO_{3-\delta}$ after sintering in air and after annealing in a reducing atmosphere versus $x$.

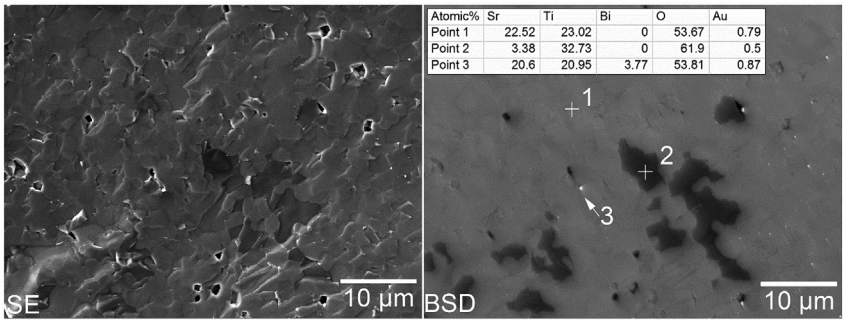


**Fig. 3.** SEM and BSD images of fracture surface of $Sr_{1-x}Bi_xTiO_{3-\delta}$ with $x = 0.01$ after annealing in a reducing atmosphere. The insert in the BSD image shows the atomic ratio of elements at three indicated points measured by EDS.

abrupt variations without any observable counterparts in the electrical conductivity measurements, except for the sample with x = 0.03 at T ~700 K. Ohta et al. [17] have shown that such transition at 750 K in heavily La-and Nb-substituted $SrTiO_3$ samples can be related to a dominant carrier scattering mechanism changing with increasing temperature from a coupled scattering by polar optical phonons and acoustic phonons to mere acoustic phonon scattering. Moreover, the samples in this study are composites with complex microstructures rather than single crystals as in Ohta's et al. study, which could be related to these variations. However, further studies (such as Hall effect measurements, magnetic measurements …) are required to understand such complex behaviour. Power factor (Fig. 4c) can be calculated from electrical conductivity and Seebeck coefficient. The power factor of $SrTiO_{3-\delta}$ is significantly improved by Bi substitution, especially at temperatures ~400 K. The highest power factor is obtained in $Sr_{1-x}Bi_xTiO_{3-\delta}$ with $x = 0.07$, ~1286 $\mu Wm^{-1}K^{-2}$ at 420 K, which is comparable with that of La and Y-doped $SrTiO_3$ at a similar doping concentration [21,43].

Fig. 4d shows that 0.5% of Bi substitution does not obviously reduce the thermal conductivity of $SrTiO_3$, whereas 5% and 7% of Bi doped $SrTiO_{3-\delta}$ and $Sr_{0.95}TiO_{3-\delta}$ exhibit reduced thermal conductivity. The reduction of the thermal conductivity in $Sr_{1-x}Bi_xTiO_{3-\delta}$ with $x = 0.05$ and 0.07 could be attributed to Bi substitution and the composite effect from Bi metal and $Ti_nO_{2n-1}$. The mass difference between $Sr^{2+}$ and $Bi^{3+}$ creates point defect scattering for phonons, thus reducing the lattice thermal conductivity. The interfaces between different phases could scatter phonons, especially the interfaces between Bi metal and the two oxides. Lyeo and Cahill have observed a low thermal conductance at the interfaces between Bi and hydrogen-terminated diamond, with a thermal conductivity approaching amorphous limit [44]. They ascribe it to the dissimilar Debye temperatures and vibrational spectra between Bi and diamond. As the Debye temperature of Bi [44] is much lower than those of $SrTiO_3$ [45] and $TiO_2$ [46], a low thermal conductivity could be expected at the interfaces between Bi and oxides. Moreover, the shear planes in $Ti_nO_{2n-1}$ can also effectively scatter phonons.

Fig. 4e shows the temperature dependence of figure of merit. *ZT* of $Sr_{1-x}Bi_xTiO_{3-\delta}$ is enhanced by substituting Sr with Bi up to $x = 0.07$, reaching ~0.13 at 1000 K. In addition, *ZT* of $Sr_{0.95}TiO_{3-\delta}$ is a little higher than that the undoped $SrTiO_3$ but much lower than that of $Sr_{0.95}Bi_{0.05}TiO_{3-\delta}$. Incorporating Bi into $SrTiO_{3-\delta}$ is beneficial for its high power factor and low thermal conductivity due to the substitution and metal inclusion, whereas a further enhancement of *ZT* in Bi-doped $SrTiO_3$ is limited by its low solubility. Therefore, Bi can be added as a co-dopant into $SrTiO_{3-\delta}$.

## 4. Conclusions

The thermoelectric properties of dense $Sr_{1-x}Bi_xTiO_{3-\delta}$ ($0 \le x \le 0.07$) and $Sr_{0.95}TiO_{3-\delta}$ ceramics prepared by solid-state reaction and conventional sintering have been studied. The presence of Bi metal and $Ti_nO_{2n-1}$ has been confirmed in $Sr_{1-x}Bi_xTiO_{3-\delta}$ ceramics, making them $Sr_{1-x}Bi_xTiO_{3-\delta}$/Bi/$Ti_nO_{2n-1}$ composites. $Ti_nO_{2n-1}$ is also observed in $Sr_{0.95}TiO_3$. The lattice parameter of $Sr_{1-x}Bi_xTiO_{3-\delta}$ increases with increasing Bi content, whereas undoped $SrTiO_{3-\delta}$ possesses the same lattice parameter as $Sr_{0.95}TiO_{3-\delta}$. It indicates that some Bi dopants are incorporated into the crystal lattice of $SrTiO_3$. Substitution of $Sr^{2+}$ with $Bi^{3+}$ increases the electrical conductivity and reduces the absolute values of Seebeck coefficient.

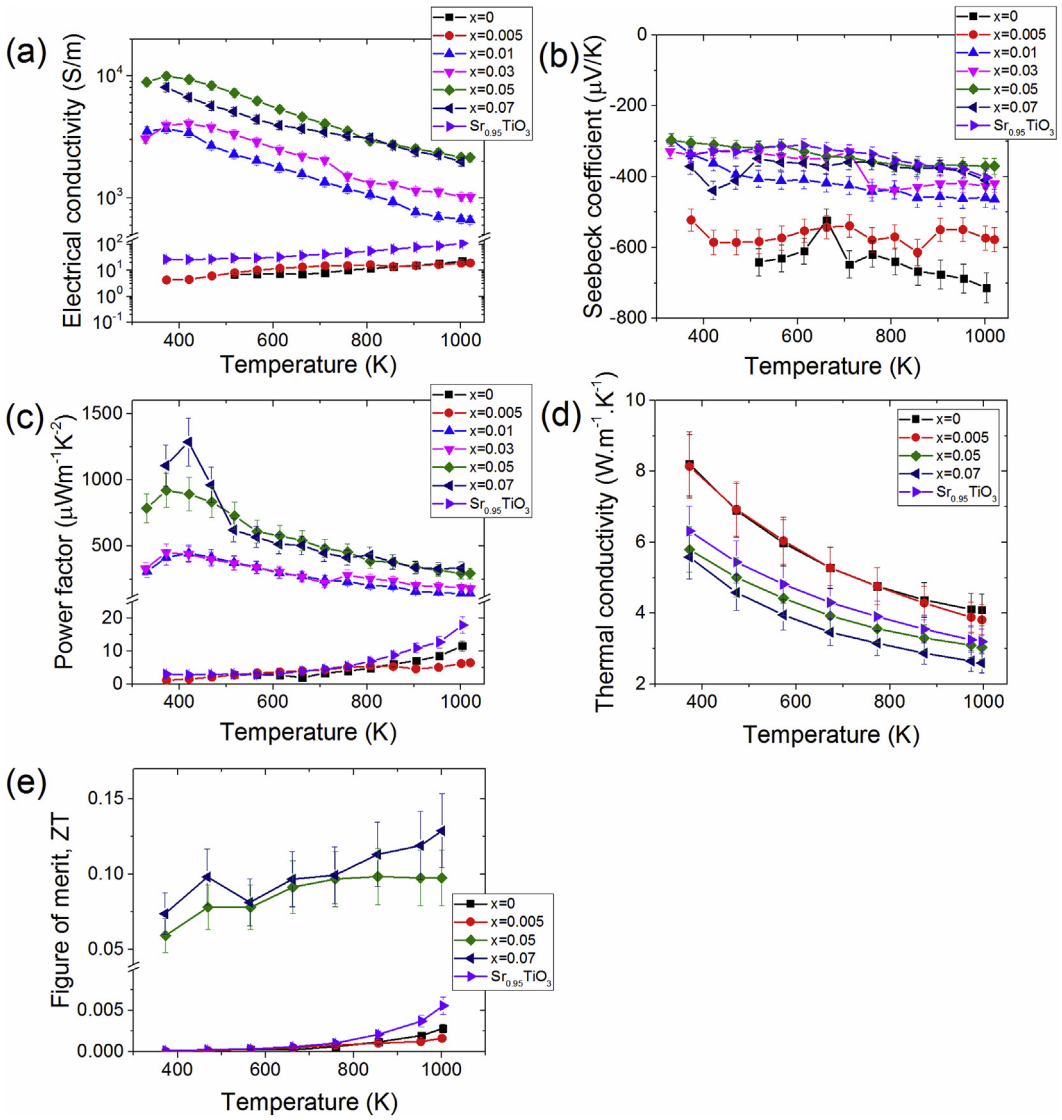


**Fig. 4.** Thermoelectric properties of $Sr_{1-x}Bi_xTiO_{3-\delta}$ ($x = 0.005$, 0.01, 0.03, 0.05, and 0.07) and $Sr_{0.95}TiO_{3-\delta}$ ceramics after annealing in a reducing atmosphere as a function of temperature. (a) Electrical conductivity, (b) Seebeck coefficient, (c) power factor, (d) thermal conductivity, and (e) figure of merit, *ZT*.

The power factor is improved in the Bi-doped samples. The thermal conductivity is effectively reduced in $Sr_{1-x}Bi_xTiO_{3-\delta}$ with $x = 0.05$ and 0.07, possibly due to the enhanced phonon scattering introduced by Bi substitution and the composite effect from Bi and $Ti_nO_{2n-1}$. Highest *ZT* ~0.13 has been achieved in $Sr_{0.93}Bi_{0.07}TiO_{3-\delta}$ at 1000 K.

## Conflicts of interest

Authors declare that there are no conflicts of interest.

## References

[1] Terasaki I, Sasago Y, Uchinokura K. Large thermoelectric power in $NaCo_2O_4$ single crystals. Phys Rev B 1997;56(20):R12685–7.
[2] Masset AC, Michel C, Maignan A, Hervieu M, Toulemonde O, Studer F, Raveau B, Hejtmanek J. Misfit-layered cobaltite with an anisotropic giant magnetoresistance: $Ca_3Co_4O_9$. Phys Rev B 2000;62(1):166–75.
[3] Shikano M, Funahashi R. Electrical and thermal properties of single-crystalline $(Ca_2CoO_3)_{0.7}CoO_2$ with a $Ca_3Co_4O_9$ structure. Appl Phys Lett 2003;82(12):1851–3.
[4] Delorme F, Martin CF, Marudhachalam P, Ovono Ovono D, Guzman G. Effect of Ca substitution by Sr on the thermoelectric properties of $Ca_3Co_4O_9$ ceramics. J Alloy Comp 2011;509(5):2311–5.
[5] Chen C, Zhang T, Donelson R, Chu D, Tian R, Tan TT, Li S. Thermopower and chemical stability of $Na_{0.77}CoO_2/Ca_3Co_4O_9$ composites. Acta Mater 2014;63:99–106.
[6] Delorme F, Chen C, Pignon B, Schoenstein F, Perriere L, Giovannelli F. Promising high temperature thermoelectric properties of dense $Ba_2Co_9O_{14}$ ceramics. J Eur Ceram Soc 2017;37(7):2615–20.
[7] Androulakis J, Migiakis P, Giapintzakis J. $La_{0.95}Sr_{0.05}CoO_3$: An efficient room-temperature thermoelectric oxide. Appl Phys Lett 2004;84(7):1099–101.
[8] Kozuka H, Yamagiwa K, Ohbayashi K, Koumoto K. Origin of high electrical conductivity in alkaline-earth doped $LaCoO_3$. J Mater Chem 2012;22(22):11003–5.
[9] Chen C, Giovannelli F, Chartier T, Delorme F. Synthesis and thermoelectric properties of doubly substituted $La_{0.95}Sr_{0.05}Co_{1-x}Cr_xO_3$ ($0 \le x \le 0.5$). Mater Res Bull 2018;102:257–61.
[10] Bousnina MA, Dujardin R, Perriere L, Giovannelli F, Guegan G, Delorme F. Synthesis, sintering, and thermoelectric properties of the solid solution $La_{1-x}Sr_xCoO_{3\pm\delta}$ ($0 \le x \le 1$). J Adv Ceram 2018;7(2):160–8.
[11] Okuda T, Nakanishi K, Miyasaka S, Tokura Y. Large thermoelectric response of metallic perovskites: $Sr_{1-x}La_xTiO_3$ ($0 \le x \le 0.1$). Phys Rev B 2001;63(11):113104.
[12] Chen C, Zhang T, Donelson R, Tan TT, Li S. Effects of yttrium substitution and oxygen deficiency on the crystal phase, microstructure, and thermoelectric properties of $Sr_{1-1.5x}Y_xTiO_{3-\delta}$ ($0 \le x \le 0.15$). J Alloy Comp 2015;629:49–54.
[13] Kovalevsky AV, Aguirre MH, Populoh S, Patrício SG, Ferreira NM, Mikhalev SM, Fagg DP, Weidenkaff A, Frade JR. Designing strontium titanate-based thermoelectrics: insight into defect chemistry mechanisms. J Mater Chem

2017;5(8):3909–22.
[14] Flahaut D, Mihara T, Funahashi R, Nabeshima N, Lee K, Ohta H, Koumoto K. Thermoelectrical properties of A-site substituted $Ca_{1-x}Re_xMnO_3$ system. J Appl Phys 2006;100(8):4.
[15] Ohtaki M, Tsubota T, Eguchi K, Arai H. High-temperature thermoelectric properties of $(Zn_{1-x}Al_x)O$. J Appl Phys 1996;79(3):1816–8.
[16] Giovannelli F, Chen C, Díaz-Chao P, Guilmeau E, Delorme F. Thermal conductivity and stability of Al-doped ZnO nanostructured ceramics. J Eur Ceram Soc 2018;38(15):5015–20.
[17] Ohta S, Nomura T, Ohta H, Koumoto K. High-temperature Carrier transport and thermoelectric properties of heavily La- or Nb-doped $SrTiO_3$ single crystals. J Appl Phys 2005;97(3):034106.
[18] Zhang L, Tosh T, Okinaka N, Akiyama T. Thermoelectric properties of combustion synthesized and spark plasma sintered $Sr_{1-x}R_xTiO_3$ (R = Y, La, Sm, Gd, Dy, 0 < x <= 0.1). Mater Trans 2007;48(8):2088–93.
[19] Liu J, Wang CL, Li Y, Su WB, Zhu YH, Li JC, Mei LM. Influence of rare earth doping on thermoelectric properties of $SrTiO_3$ ceramics. J Appl Phys 2013;114(22).
[20] Dehkordi AM, Bhattacharya S, He J, Alshareef HN, Tritt TM. Significant enhancement in thermoelectric properties of polycrystalline Pr-doped $SrTiO_3$-delta ceramics originating from nonuniform distribution of Pr dopants. Appl Phys Lett 2014;104(19).
[21] Chen C, Zhang T, Donelson R, Tan TT, Li S. Effects of yttrium substitution and oxygen deficiency on the crystal phase, microstructure, and thermoelectric properties of $Sr_{1-1.5x}Y_xTiO_{3-\delta}$ ($0 \le x \le 0.15$). J Alloy Comp 2015;629:49–54.
[22] Wang HC, Wang CL, Su WB, Liu J, Sun Y, Peng H, Mei LM. Doping effect of La and Dy on the thermoelectric properties of SrTiO3. J Am Ceram Soc 2011;94(3):838–42.
[23] Kovalevsky AV, Yaremchenko AA, Populoh S, Weidenkaff A, Frade JR. Effect of A-site cation deficiency on the thermoelectric performance of donor-substituted strontium titanate. J Phys Chem C 2014;118(9):4596–606.
[24] Bhattacharya S, Dehkordi AM, Tennakoon S, Adebisi R, Gladden JR, Darroudi T, Alshareef HN, Tritt TM. Role of phonon scattering by elastic strain field in thermoelectric $Sr_{1-x}Y_xTiO_{3-delta}$. J Appl Phys 2014;115(22).
[25] Zhang B, Wang J, Zou T, Zhang S, Yaer X, Ding N, Liu C, Miao L, Li Y, Wu Y. High thermoelectric performance of Nb-doped $SrTiO_3$ bulk materials with different doping levels. J Mater Chem C 2015;3(43):11406–11.
[26] Lu Z, Zhang H, Lei W, Sinclair DC, Reaney IM. High-Figure-of-Merit thermoelectric La-doped A-site-deficient $SrTiO_3$ ceramics. Chem Mater 2016;28(3):925–35.
[27] Srivastava D, Norman C, Azough F, Schäfer MC, Guilmeau E, Freer R. Improving the thermoelectric properties of $SrTiO_3$-based ceramics with metallic inclusions. J Alloy Comp 2018;731:723–30.
[28] Park K, Son JS, Woo SI, Shin K, Oh M-W, Park S-D, Hyeon T. Colloidal synthesis and thermoelectric properties of La-doped $SrTiO_3$ nanoparticles. J Mater Chem 2014;2(12):4217–24.
[29] Wang N, Chen H, He H, Norimatsu W, Kusunoki M, Koumoto K. Enhanced thermoelectric performance of Nb-doped $SrTiO_3$ by nano-inclusion with low thermal conductivity. Sci Rep 2013;3.
[30] Wang J, Zhang B-Y, Kang H-J, Li Y, Yaer X, Li J-F, Tan Q, Zhang S, Fan G-H, Liu C-Y, Miao L, Nan D, Wang T-M, Zhao L-D. Record high thermoelectric performance in bulk $SrTiO_3$ via nano-scale modulation doping. Nano Energy 2017;35:387–95.
[31] Ohta H, Kim S, Mune Y, Mizoguchi T, Nomura K, Ohta S, Nomura T, Nakanishi Y, Ikuhara Y, Hirano M. Giant thermoelectric Seebeck coefficient of a two-dimensional electron gas in $SrTiO_3$. Nat Mater 2007;6(2):129–34.
[32] Lee KH, Kim SW, Ohta H, Koumoto K. Ruddlesden-Popper phases as thermoelectric oxides: Nb-doped $SrO(SrTiO_3)_n$ (n= 1, 2). J Appl Phys 2006;100(6):063717.
[33] Wang Y, Wan C, Zhang X, Shen L, Koumoto K, Gupta A, Bao N. Influence of excess SrO on the thermoelectric properties of heavily doped $SrTiO_3$ ceramics. Appl Phys Lett 2013;102(18):183905.
[34] Gong C, Dong G, Hu J, Chen Y, Qin M, Yang S, Gao F. Effect of reducing annealing on the microstructure and thermoelectric properties of La–Bi co-doped SrTiO3 ceramics. J Mater Sci Mater Electron 2017;28(19):14893–900.
[35] Rodríguez-Carvajal J. Recent developments of the program FULLPROF. Comm Powder Diffr (IUCr). Newsletter 2001;26:12–9.
[36] Boston R, Schmidt WL, Lewin GD, Iyasara AC, Lu Z, Zhang H, Sinclair DC, Reaney IM. Protocols for the fabrication, characterization, and optimization of n-type thermoelectric ceramic oxides. Chem Mater 2017;29(1):265–80.
[37] Shannon R. Revised effective ionic radii and systematic studies of interatomic distances in halides and chalcogenides. Acta Crystallogr A 1976;32(5):751–67.
[38] Shimakawa Y, Kubo Y. Degradation of ferroelectric $SrBi_2Ta_2O_9$ materials under reducing conditions and their reaction with Pt electrodes. Appl Phys Lett 1999;75(18):2839–41.
[39] Blennow P, Hansen KK, Reine Wallenberg L, Mogensen M. Effects of Sr/Ti-ratio in $SrTiO_3$-based SOFC anodes investigated by the use of cone-shaped electrodes. Electrochim Acta 2006;52(4):1651–61.
[40] Harada S, Tanaka K, Inui H. Thermoelectric properties and crystallographic shear structures in titanium oxides of the Magnèli phases. J Appl Phys 2010;108(8):083703.
[41] Portehault D, Maneeratana V, Candolfi C, Oeschler N, Veremchuk I, Grin Y, Sanchez C, Antonietti M. Facile general route toward tunable Magnéli nanostructures and their use as thermoelectric metal oxide/carbon nanocomposites. ACS Nano 2011;5(11):9052–61.
[42] Spinelli A, Torija MA, Liu C, Jan C, Leighton C. Electronic transport in doped $SrTiO_3$: Conduction mechanisms and potential applications. Phys Rev B 2010;81(15):155110.
[43] Liu J, Wang CL, Su WB, Wang HC, Zheng P, Li JC, Zhang JL, Mei LM. Enhancement of thermoelectric efficiency in oxygen-deficient $Sr_{1-x}La_xTiO_{3-\delta}$ ceramics. Appl Phys Lett 2009;95(16):162110.
[44] Lyeo H-K, Cahill DG. Thermal conductance of interfaces between highly dissimilar materials. Phys Rev B 2006;73(14):144301.
[45] Duran A, Morales F, Fuentes L, Siqueiros JM. Specific heat anomalies at 37, 105 and 455 K in $SrTiO_3$: Pr. J Phys Condens Matter 2008;20(8).
[46] Traylor JG, Smith HG, Nicklow RM, Wilkinson MK. Lattice dynamics of rutile. Phys Rev B 1971;3(10):3457–72.

**Dr. C. Chen** was a post-doctor in GREMAN laboratory, University of Tours, France, from 2015 to 2017. She currently works as an Adolf-Martens fellow in Bundesanstalt für Materialforschung und –prüfung, Germany. She obtained her PhD under the supervision of Prof. Sean Li from the University of New South Wales (UNSW), Australia, in 2015. She was awarded a double Bachelor's degree from UNSW and Nankai University, China. Her research focuses on the synthesis and characterization of thermoelectric oxides and micro non-destructive testing by X-ray refraction.

**Dr. M.A. Bousnina** occupies a Postdoctoral position at the Process and Materials Science Laboratory, University of Paris 13, France, in NINO research group. He received his PhD degree in Chemistry in 2013 from University of Paris 13, directed by Prof. N. Jouini. He worked as a Postdoctoral fellow in GREMAN Laboratory from 2015 to 2016. His research activity is focused on solid-state chemistry, especially the synthesis and properties study of oxide materials. He rejoined the University of Paris 13 from 2016 to 2018 as temporarily attached to education and research. The objectives of the research are synthesis in Polyol media and magnetic characterization of $MFe_2O_4$ with M = Zn and Ni.

**Dr. F. Giovannelli** received his PhD degree in Material Sciences from Caen University in 2002, and has been an assistant professor at University of Tours since 2005. He is in charge of the research group "Functional oxides for energy efficiency" of GREMAN Laboratory. His research activity is focused on solid state chemistry, especially the synthesis and characterization of oxide materials with remarkable properties (thermoelectrics, piezoelectrics, superconductors, …). The objectives of the research undertaken are the understanding of all the mechanisms which control properties in oxides and their correlation with chemistry or manufacturing process for devices or applications referred to energy transport, storage, conversion or saving.

**Dr. F. Delorme** is Senior Researcher in GREMAN laboratory, University of Tours, France. He obtained his Ph.D. in Materials Chemistry in 2002 from University of Caen, (France) in CRISMAT laboratory, directed by Prof. B. Raveau. He worked in BRGM (French Geological Survey) from 2002 to 2008 and in Corning from 2008 to 2010, as the research group leader. He joined GREMAN laboratory as Senior Researcher in 2011. His research focuses on materials for energy efficiency, their synthesis, sintering, characterization, and applications, with a particular focus on piezoelectric and thermoelectric oxides.